

Article

Physical, Rheological, and Anti-Ultraviolet Aging Performance of Layered Double Hydroxides + Styrene Block Copolymer-Modified Asphalt Binders

Yu Song ¹, Shaopeng Wu ^{1,*}, Anqi Chen ¹ and Yuanyuan Li ² 

¹ State Key Laboratory of Silicate Materials for Architectures, Wuhan University of Technology, Wuhan 430070, China; songiyy@whut.edu.cn (Y.S.); anqi.chen@whut.edu.cn (A.C.)

² School of Civil Engineering and Architecture, Wuhan Institute of Technology, Wuhan 430072, China; liyy@wit.edu.cn

* Correspondence: wusp@whut.edu.cn

Abstract: To determine the preparation parameters of layered double hydroxides (LDHs) + styrene butadiene styrene block copolymer (SBS)-modified asphalt binders (MABs) in engineering applications and identify the structure of LDHs used in asphalt modification, this paper investigated the physical, rheological, and UV aging resistance of LDHs + SBS MABs under various preparation parameters. Fourier transform infrared spectroscopy (FTIR), X-ray diffraction (XRD), scanning electron microscopy (SEM), and an ultraviolet-visible spectrophotometer (UV-vis) were used to characterize the structure and UV resistance of LDHs and D-LDHs (dissolving from LDHs + SBS MABs). The mechanical properties of LDHs + SBS MABs were studied based on penetration, ductility, softening point, and rotational viscosity tests. The rheological performance and UV aging resistance of LDHs + SBS MABs were assessed using the bending beam rheometer (BBR) test, direct tensile test (DTT), dynamic shear rheometer (DSR) test, and FTIR. The results demonstrated that the crystal and chemical structures of LDHs remain unchanged before and after use in asphalt modification. The optimal preparation parameters of LDHs + SBS MABs were as follows: a preparation temperature of 170 °C, a shearing time of 60 min, and a shearing rate of 4000 r/min. The high-temperature performance of LDHs + SBS MABs improved significantly with LDHs added, and the low-temperature performance slightly decreased. The viscosity of LDHs + SBS MABs with 4 wt% LDHs at 135 °C was 1.920 Pa·s, which was 47.4% higher than that of SBS MABs. The DTT results indicated that SBS MABs have the highest fracture energy (FE) value of 4873 J/m², showing the best low-temperature cracking resistance. In comparison, the FE values of MABs doped with 3 wt% and 4 wt% LDHs are 4518 J/m² and 4248 J/m², respectively, just 7.3% and 12.8% lower than that of ABs without LDHs. The complex modulus aging index (CMAI) of MABs doped with 4% LDHs is 14.3%, which is 15.9% lower than that of SBS MABs, indicating that the anti-ultraviolet aging performance of LDHs + SBS MABs has been improved. FTIR analysis demonstrated that the relative content of C=O (RCC) and S=O (RCS) of LDHs + SBS MABs decreased drastically compared with SBS MABs, indicating that the UV aging resistance of LDHs + SBS MABs was largely enhanced. Furthermore, the segregation test result of 3wt% LDHs + SBS-modified asphalt is 0.3 °C, showing the best compatibility with asphalt.

Keywords: LDHs + SBS-modified asphalt; preparation parameters; rheological performance; anti-UV aging performance



Citation: Song, Y.; Wu, S.; Chen, A.; Li, Y. Physical, Rheological, and Anti-Ultraviolet Aging Performance of Layered Double Hydroxides + Styrene Block Copolymer-Modified Asphalt Binders. *Sustainability* **2023**, *15*, 15246. <https://doi.org/10.3390/su152115246>

Academic Editors: Rui Micaelo, Rosolino Vaiana and Ramadhansyah Putra Jaya

Received: 1 August 2023

Revised: 11 September 2023

Accepted: 28 September 2023

Published: 25 October 2023



Copyright: © 2023 by the authors. Licensee MDPI, Basel, Switzerland. This article is an open access article distributed under the terms and conditions of the Creative Commons Attribution (CC BY) license (<https://creativecommons.org/licenses/by/4.0/>).

1. Introduction

Asphalt is a sort of extensively used road-building material [1–4]. Styrene butadiene styrene block copolymer (SBS)-modified asphalt binders (MABs) have a superior high- and low-temperature performance and are often applied in highway pavement construction [5,6]. Nevertheless, the coupling effects of moisture [7], heat [8], and light [9] will influence the road performance of the asphalt pavement during its service [10,11]. Among

these factors, the ultraviolet (UV) aging of asphalt caused by UV irradiation heavily deteriorates the rheological properties of SBS MABs and seriously endangers traffic safety [12,13]. Hence, it is significant and urgent to heighten the UV aging resistance of SBS MABs to extend the service life of pavements for fitting sustainable road development concepts [14,15].

Anti-UV aging agents, including UV absorbers [16], inorganic nanoparticles [17,18], and layered silicates [19,20], were therefore introduced into SBS MABs to ameliorate the UV aging resistance of asphalt. Liu et al. [16] argued that UV absorbers greatly influence the phase angle and viscoelasticity of SBS MABs and can effectively inhibit their aging. However, the structure of SBS modifiers predominantly affects the effect of UV absorbers. Moreover, nanomaterials, such as Al₂O₃ nanoparticles [17], were then applied to the modification of SBS MABs, and both the high-temperature and anti-UV aging performances of the specimens were enhanced. Similarly, the addition of the CeO₂ nanoparticles ameliorated the complex modulus and high-temperature performance of the ABs and enhanced the UV aging resistance, but the modification effect was less significant [18]. Li et al. [20] showed that the 4 wt% montmorillonite (MMT) MAB owns excellent anti-UV aging properties. Nevertheless, inorganic additives, including montmorillonite and carbon black, had a hardening effect when used in asphalt modification, leading to the performance deterioration of ABs at low temperatures [21].

Layered double hydroxide (LDH) is a layered material with a supramolecular structure [22]. Studies [23,24] have shown that LDHs can heighten the anti-UV aging performance of ABs, which is attributed to their unique structure that provides physical shielding and chemical absorption of UV light [18]. Zhang et al. [25] showed that dodecyltrimethoxysilane surface organic modified LDHs (OLDHs) were significantly more compatible with SBS MABs than LDHs, and the OLDH-modified SBS MABs exhibit a superior high-temperature performance and UV aging resistance.

Other organic anionic modifiers, such as sodium dodecyl sulfate (SDS) [26] and sodium stearate (SS), whose main chains consist of 12 and 18 carbon atoms, respectively, were also utilized in LDH modification. They can increase the compatibility of LDHs with ABs and heighten the anti-UV aging performance of OLDH MABs. Furthermore, LDHs can improve the road performance of asphalt mixtures [23]. Zhao et al. [27] concluded that adding LDHs can significantly heighten the resistance to water damage and freeze–thaw splitting of UV-aged SBS MA mixtures and thus enhances their high-temperature and long-term low-temperature properties. Li et al. [28] reclaimed LDHs + SBS MABs from a test road and SBS MABs from a comparison road after several years of service. They investigated the rheological and aging properties of the specimens with a Fourier infrared spectrometer (FTIR) and a dynamic shear rheometer (DSR). The results demonstrated that the LDHs decreased surface asphalt concrete's aging rate and the aging's diffusion rate into the interior of asphalt pavements. Therefore, the practical application of LDHs as an anti-aging agent is scientific and feasible.

It is a critical issue to determine the preparation technology of LDH MABs and the dosage of LDHs in the engineering application of LDHs. Melt blending is an efficient and straightforward method to prepare LDH MABs [29]. At the same time, preparation parameters, including the modifier dosage, preparation temperature, shear time, and shear rate, have a remarkable effect on the dispersion of modifiers in ABs [30]. Zhang et al. [31] proposed that LDHs could enhance ABs' UV aging resistance, and the modification effect was enhanced with increases in LDHs. A study [32] showed that LDHs containing carbonate ions could reduce the negative impact of UV aging on ABs, especially when their content achieved more than 3 wt%. And Wang et al. [33] prepared LDH MABs with different preparation parameters based on this. They concluded that the distribution of LDH particles in asphalt is small and uniform with a shearing rate of 3000 r/min, shearing time of 60 min, and additive amount of 3 wt% for the LDHs. Thus, Yang et al. [29] summarized the specific process parameters of most research in preparing layered clay MABs. That is, the modifier content is generally 4 ± 2 wt%, the preparation temperature is mainly 155 ± 15 °C, the shearing time is more than 60 min, and the shearing rate is

about 4000 r/min. Xu et al. [34] then prepared LDH MABs with different LDH contents via melting at 150 °C with a shear rate of 4000 r/min and a shear time of 60 min. The results of the physical properties and aging index of LDH MABs indicated that it was better to control the content of LDHs within 5 wt%. Overall, the determination of the production parameters of LDH MABs is highly relevant to their physical properties. However, studies on determining the suitable preparation parameters of LDH MABs and optimal dosage of LDHs for asphalt binders from specific sources are still insufficient.

This paper investigated the physical properties, high-temperature storage stability, and viscosity of LDH MABs prepared with different preparation parameters and the distribution state of SBS in ABs to optimize the best preparation parameters. Then, LDH MABs with varied LDH contents (0 wt%, 3 wt%, and 4 wt%) were prepared under the optimal preparation parameters. All specimens were subjected to UV aging under the same conditions to investigate the effects of UV aging on the physical properties, viscosity, rheological properties, and anti-UV aging performance of LDH MABs.

2. Materials and Methods

2.1. Raw Materials

An SBS MAB (Performance Grade 58-22) from Sichuan Shuwu Pavement Material Co., Ltd. (Guang'an, China) was applied as the primary binder, the properties of which are displayed in Table 1. The SBS MAB has a good high- and low-temperature performance, with a softening point of 65.3 °C and a ductility (15 °C) of 63.8 cm.

Table 1. Properties of SBS MAB.

Properties	Results	Methods [35]
Penetration (25 °C, 100 g, 5 s; 0.1 mm)	90.1	T 0604
Softening point (°C)	65.3	T 0606
Ductility (15 °C; cm)	63.8	T 0605
Viscosity (135 °C; Pa·s)	1.293	T 0625

LDHs from GCH Technology CO., Ltd. (Guangzhou, China) were used as an anti-UV aging modifier. An X-ray fluorescence spectrometer (XRF) test was applied to study the chemical composition of the LDHs; the results are shown in Table 2. As can be seen from Table 2, the main chemical compositions of the LDHs are CO₂, MgO, and Al₂O₃.

Table 2. Chemical compositions of LDHs.

Chemical Compositions	CO ₂	Na ₂ O	MgO	Al ₂ O ₃	SiO ₂	SO ₃	Cl	CaO	ZnO
Weight (%)	44.203	0.105	33.344	22.199	0.015	0.011	0.017	0.099	0.007

2.2. Experimental Methods

2.2.1. Preparation of LDH MABs

The 4 wt% LDHs were mixed with the heated SBS MABs using a high-speed shearing apparatus (500 r/min, 30 min) to confirm the dispersion uniformity of LDHs in ABs. The LDHs + SBS MABs were then sheared at a high shearing rate (4000 r/min, 5000 r/min) for different times (60 min, 90 min). For better comparison, the SBS MABs without LDHs underwent the same preparation process as ABs with LDHs. The preparation parameters are displayed in Table 3.

Table 3. Preparation parameters.

Sample	Shear Temperature (°C)	Shear Time (min)	Shear Rate (r/min)
1	170	60	4000
2	160	60	4000
3	170	90	4000
4	170	60	5000

2.2.2. Reclaiming of LDHs

The LDHs were filtered out from the solution of carbon tetrachloride (CCl₄) and the LDHs + SBS MABs. They were washed with CCl₄ until the filtrate was clear then dried and ground into powder. The dissolved LDHs (D-LDHs) were finally obtained.

2.2.3. Characterization of LDHs and D-LDHs

The chemical structure of LDHs and D-LDHs was determined via FTIR with a wavenumber of 4000–400 cm⁻¹. An XRD test, with Cu-k α radiation of 1.540 Å, a working voltage of 40 kV, and 2 θ ranging from 5° to 80° (5°/min), was conducted to determine the crystalline structure of LDHs and D-LDHs. Scanning electron microscopy (SEM) was utilized to investigate the surface morphology of LDHs and D-LDHs with an acceleration voltage of 15 kV. An ultraviolet-visible spectrophotometer (UV-vis), Lambda 750 S (PerkinElmer, America), was applied to investigate the samples' absorption and reflection spectra via UV-vis with a wavelength of 200–2500 nm.

2.2.4. UV Aging Simulation Tests

UV aging simulation tests include thermo-oxidative aging (volatilization) in the short term and UV aging in the long term. The former was conducted in the form of thin film oven tests (TFOTs), which were conducted at 163 °C for 5 h (T 0610) [35]. Then, the specimens were placed in a UV aging oven for 7 d with a UV light intensity of 1200 μ W/cm².

2.2.5. Evaluation of UV Aging Resistance

The penetration retention rate (PRR) softening point increment (SPI); viscosity aging index (VAI); difference in softening point between the top and bottom samples (ΔT); and complex modulus-based aging index (CMAI) are utilized to evaluate unaged and UV-aged ABs, as shown in Equations (1)–(5).

$$\text{PRR} = \frac{P_2}{P_1} \times 100\% \quad (1)$$

$$\text{SPI} = SP_2 - SP_1 \quad (2)$$

$$\text{VAI} = \frac{V_1 - V_2}{V_1} \times 100\% \quad (3)$$

where P_1 , SP_1 , and V_1 represent the penetration, softening point, and viscosity before UV aging and P_2 , SP_2 , and V_2 represent those after UV aging.

$$\Delta T = T_1 - T_2 \quad (4)$$

where T_1 corresponds to the softening point of the sample in the top section and T_2 corresponds to that in the bottom section. (The aluminum tube was cut evenly into three sections, with the anodized flats taken from the top and bottom of the tube, respectively.)

$$\text{CMAI} = \frac{G_2^* - G_1^*}{G_1^*} \times 100\% \quad (5)$$

where G_1^* represents the initial complex modulus of unaged Abs and G_2^* represents the initial complex modulus of aged ABs.

FTIR was conducted to evaluate the chemical structure of unaged and UV-aged ABs. The 5% mass fraction of the asphalt was dissolved in C_2S to form the solution, a drop of which was then put on a KBr slide, dried, and tested.

The low-temperature performance of the unaged and UV-aged ABs was studied using a bending beam rheometer (BBR) and the direct tensile test (DTT). The BBR tests used test temperatures ($-12\text{ }^\circ\text{C}$, $-18\text{ }^\circ\text{C}$) and a test load of $980 \pm 50\text{ mN}$. DTTs applied a stretching rate of 1 mm/min and a test temperature of $-20\text{ }^\circ\text{C}$. The intermediate performance of the unaged and UV-aged ABs was studied using the dynamic shear rheometer (DSR) test. The test applied a rotor diameter of 25 mm and a temperature from $52\text{ to }82\text{ }^\circ\text{C}$ ($2\text{ }^\circ\text{C/min}$, 10 rad/s). And the high-temperature performance of ABs was studied using a viscometer. Figure 1 is the technical roadmap of this paper.

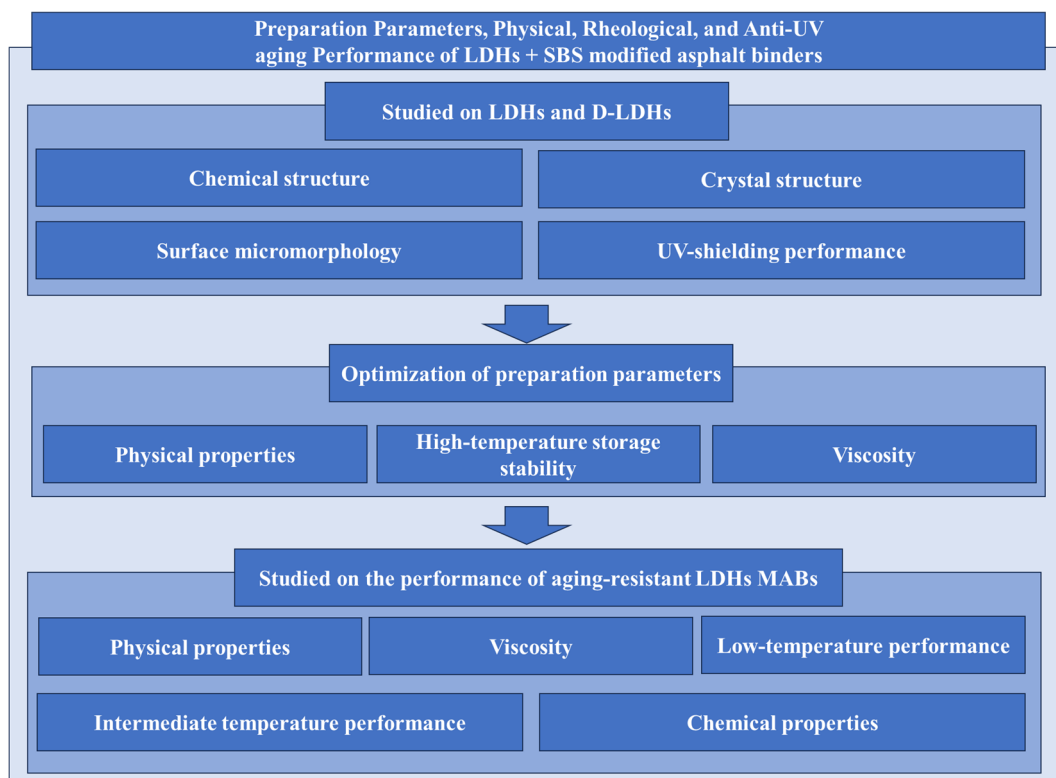


Figure 1. Technical roadmap of this paper.

3. Results and Discussions

3.1. Structure and Performance Characterization of LDHs and D-LDHs

3.1.1. Chemical Structures of LDHs and D-LDHs

FTIR is an efficient method for detecting chemical structure changes in asphalt [36,37]. Figure 2 shows the FTIR spectrogram of LDHs and D-LDHs, and the characteristic peaks in the spectra of the two are highly consistent, which means that the chemical structure of LDHs has not changed after use in asphalt modification. In the high wavenumber region of Figure 2, the absorption peak at 3677 cm^{-1} is generated by the vibrations of free hydroxyl ($-\text{OH}$) groups on the surface of LHDs, and that with a broader peak shape at 3446 cm^{-1} is produced by the stretching vibrations of $-\text{OH}$ in the water molecule. The peaks ranging from $3000\text{ to }2800\text{ cm}^{-1}$ are generated by the vibration of $-\text{CH}_3$ and $-\text{CH}_2$, which are introduced by the organic substance in LDH preparation. Another characteristic peak at 1359 cm^{-1} is produced by the stretching vibration of CO_3^{2-} in the metal layer of LDHs and D-LDHs. In the lower wavenumber region ($400\text{--}800\text{ cm}^{-1}$), the characteristic peaks are generated by the interaction between Mg^{2+} , Al^{3+} , and O^{2-} (Mg-O , Al-O , and Mg-O-Mg) in

the metal hydroxide layers of the LDH and D-LDH lattice. Overall, the spectra of LDHs and D-LDHs have no noticeable differences. Both reflect the characteristic functional groups of LDHs, indicating that no structural changes occur before and after LDHs are used in asphalt modification. This means that LDHs have an adequate performance stability when used in asphalt modification.

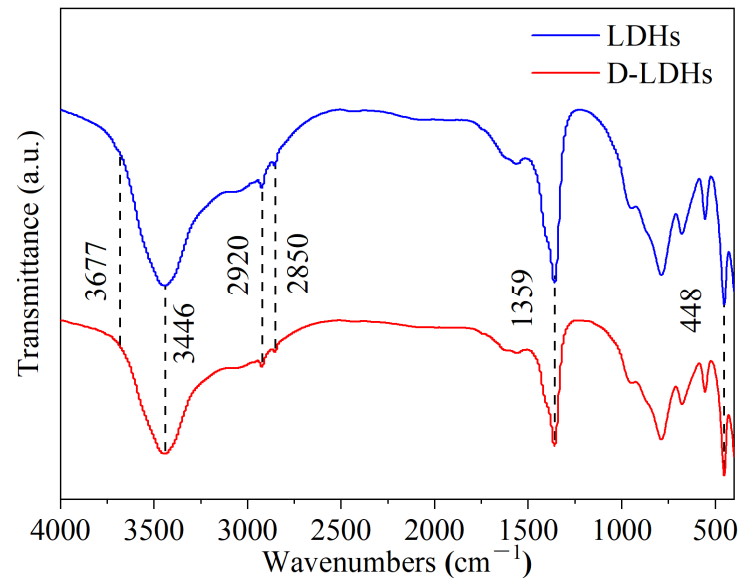


Figure 2. FTIR spectra of LDHs and D-LDHs.

3.1.2. Crystal Structures of LDHs and D-LDHs

The crystalline structures of LDHs and D-LDHs were investigated using an XRD test, and the results are shown in Figure 3. In the low angular region, three sharp diffraction peaks are presented for both LDHs and D-LDHs, corresponding to the (003), (006), and (012) crystal faces of LDH crystals, which are related to the LDHs' layered structure. The overall patterns of LDHs and D-LDHs indicate that the crystal structure of LDHs remains unchanged before and after mixing with asphalt binders. Hence, mechanical mixing under the specific preparation parameters will not destroy the crystal structure of LDHs owing to their stable chemical properties.

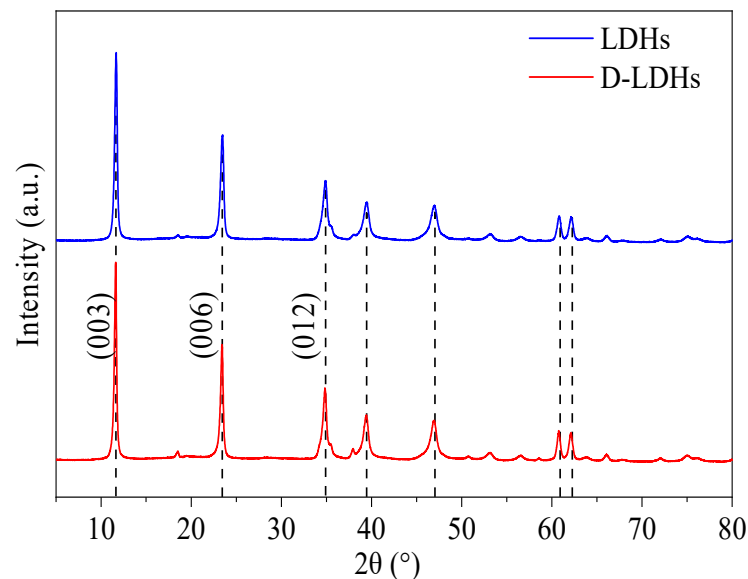


Figure 3. XRD spectra of LDHs and D-LDHs.

3.1.3. Surface Micromorphology of LDHs and D-LDHs

The surface micromorphology of LDHs before and after their use in asphalt modification is presented in Figure 4. The SEM images of LDHs (Figure 4a,b) and D-LDHs (Figure 4c,d) show that the fine lamellar particles within LDHs and D-LDHs have smooth surfaces and a uniform size distribution, which is beneficial to their dispersion in ABs. These lamellar particles are stacked in a particular direction within a small area, forming the layered structure of LDHs. The SEM results generally present a highly consistent surface micromorphology of the LDHs and D-LDHs, demonstrating that the microstructural characteristics of the LDHs dissolved from the binder have not changed.

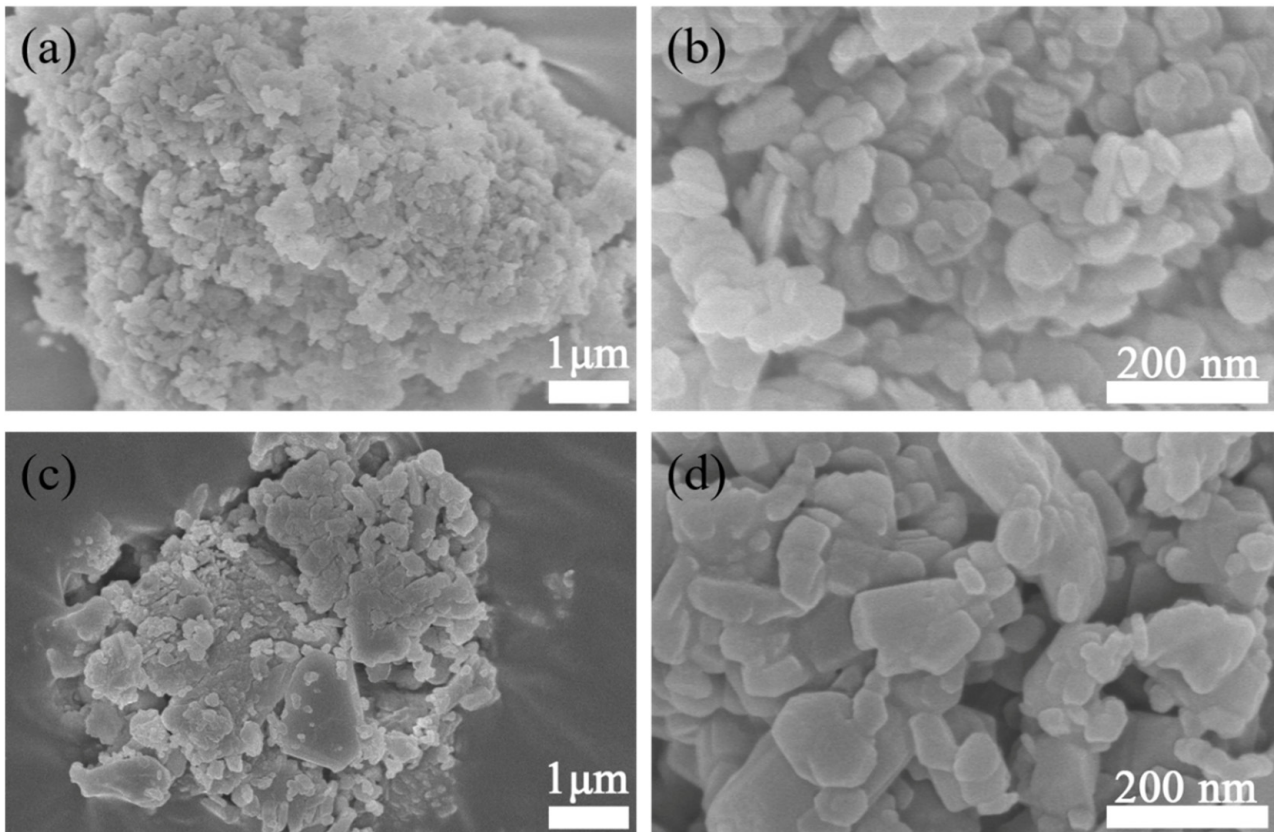


Figure 4. SEM images of LDHs and D-LDHs ((a) LDHs, 10,000 \times ; (b) LDHs, 50,000 \times ; (c) D-LDHs, 10,000 \times ; (d) D-LDHs, 50,000 \times).

3.1.4. The UV-Shielding Properties of LDHs

The UV-shielding properties of the LDHs were studied using a UV-vis spectrophotometer. The UV-vis test results are displayed in Figure 5, which contains two curves, the absorbance and reflectivity of LDHs. As can be seen from the graph, when the test light wavelength is 300–400 nm the absorbance of LDHs is around 0.14, indicating that the LDHs have a relatively strong absorption effect on UV light. Meanwhile, the reflectivity of LDHs to incident light reaches higher than 70% when the wavelength of the test light ranges from 250 to 400 nm. Since asphalt pavements are mainly irradiated by UV light in the medium wavelength range (280–400 nm) during service [38], the UV-vis test results demonstrate that LDHs have superior UV light-blocking properties. Thus, mechanical stirring at the preparation temperature facilitates the dispersion of LDHs in ABs and ensures the effect of UV shielding.

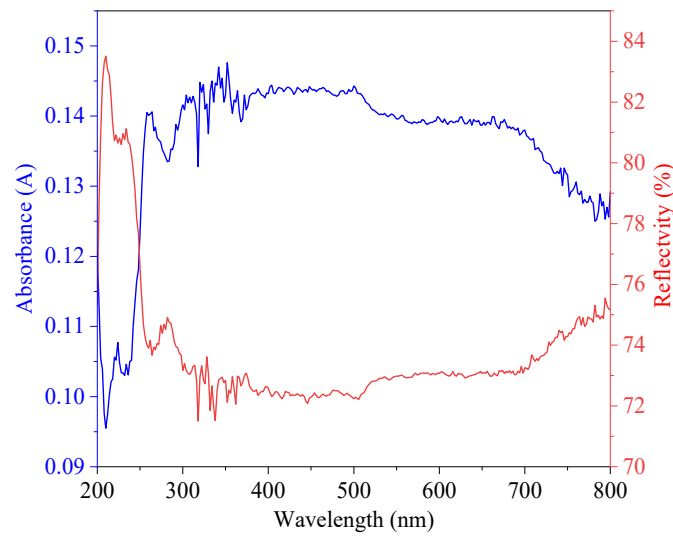


Figure 5. The UV-vis results of LDHs.

3.2. Investigation of the Preparation Parameters of LDH MABs

3.2.1. Effect of Preparation Parameters on the Physical Properties of LDH MABs

Figure 6 details the influence of preparation parameters, including the temperature, shear time, and shear rate, on the physical properties of LDH MABs. As shown in Figure 5, the softening point of LDHs + SBS MABs obtained under different preparation parameters increases largely, while the low-temperature performances of the binders drop partially. Different preparation parameters significantly influence the ductility of LDH MABs but have little influence on the softening point and penetration.

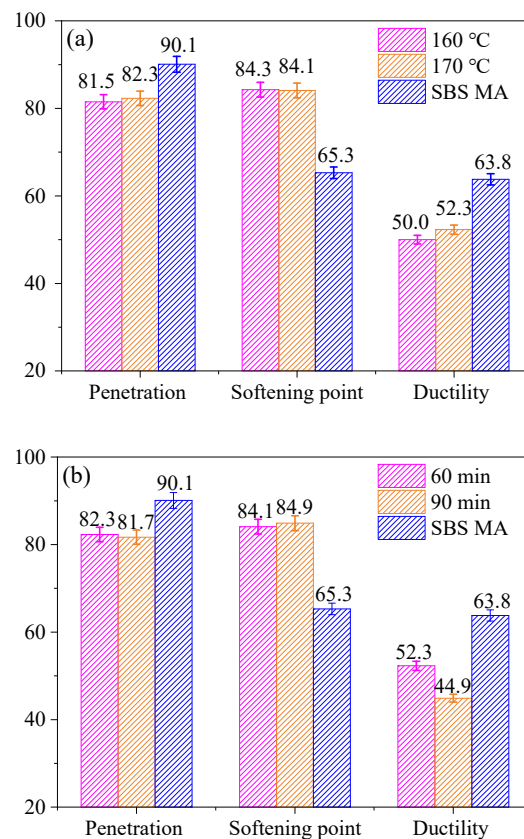


Figure 6. Cont.

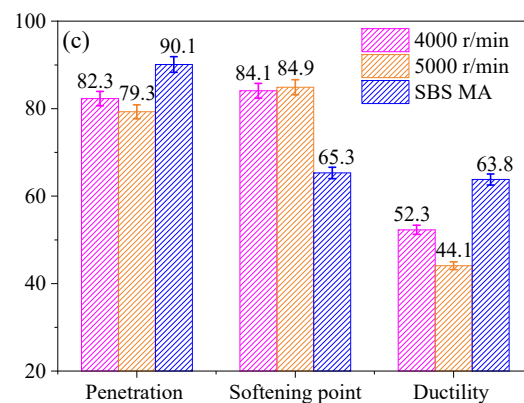


Figure 6. Effect of preparation parameters ((a) temperature, (b) time, (c) shearing rate) on 25 °C penetration, softening point, and 15 °C ductility of LDH MABs.

Figure 6a shows the influence of preparation temperatures on the physical properties of MABs with different LDH contents. The difference between the penetration and softening point of the samples at 160 °C and 170 °C, which are 0.08 mm and 0.2 °C, respectively, is relatively small. However, the ductility values at 160 and 170 °C are 50.0 and 52.3 cm, respectively, a difference of 2.3 cm. This is because the ABs' viscosity is lower at the higher temperature (170 °C), which improves the dispersion uniformity of LDHs in SBS MABs.

In Figure 6b, the ductility of the LDH MABs was 52.3 cm at the shearing time of 60 min, an increase of 16.5% compared to 44.9 cm at 90 min. Similarly, in Figure 6c, the ductility of the LDH MABs at the shearing rate of 4000 r/min increases by 18.6% compared to that of 5000 r/min. Essentially, the reason is that a too long shearing time or too high shearing rate may cause the aggregation of LDHs in SBS MABs. Therefore, this paper uses a temperature of 170 °C, a shearing time of 60 min, and a shearing rate of 4000 r/min as the best preparation parameters.

3.2.2. Effect of Preparation Parameters on the High-Temperature Storage Stability and Viscosity of LDH MABs

The results of the high-temperature storage stability tests for MABs (under the optimal preparation parameters) with different LDH doses are displayed in Figure 7. The ΔT of LDH MABs with 0 wt%, 3 wt%, and 4 wt% LDH contents are 1.6 °C, 0.3 °C, and 1.9 °C, respectively, all of which meet the requirement of being no higher than 2.5 °C in the technical specifications for asphalt pavement construction of China.

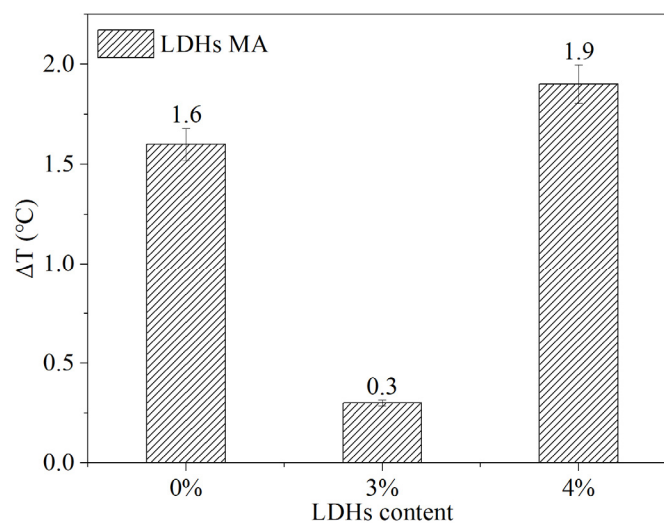


Figure 7. High-temperature storage stability of LDH MABs.

Owing to the high-temperature (163 °C) condition in the test, the SBS MAB is in a completely liquid state with a low viscosity. Meanwhile, the density of the SBS modifier is smaller than that of the AB, which makes the SBS severely disintegrate in the specimens without LDHs. And the uplifting of SBS leads to a high softening point of the top binder, resulting in a high ΔT of 1.6 °C. In comparison, the sample with 3 wt% LDHs shows the most remarkable modification effect with the ΔT of 0.3 °C, decreasing by 81.3% compared to the binders without LDHs. This is mainly caused by the fact that the LDH powder can be uniformly dispersed in the SBS MABs, increasing the system's viscosity and hindering the uplift of SBS. Hence, the difference in the softening point between the top and bottom specimens is minimal, and the storage stability of the LDH MABs is optimal. However, the LDHs and asphalt are hydrophilic and lipophilic substances, respectively. The compatibility between them worsens with a higher content (4 wt%) of LDHs, resulting in the poor storage stability of the LDH MABs with the ΔT of 1.9 °C.

Figure 8 presents the viscosity of LDH MABs at 135 °C and 175 °C for different LDH doping levels. It can be seen from the graph that LDH MABs' viscosity is higher than that of SBS MABs, and the viscosity increases with the addition of LDHs. The viscosity values of LDH MABs with 4 wt% LDHs at 135 and 175 °C are 1.920 and 0.004 Pa·s, respectively, which are 0.617 and 0.003 Pa·s higher than that of SBS MABs. The main reason is that the LDH particles dispersed in the MABs have a strong hindering effect on the movement of the asphalt molecules and can efficiently heighten the rheological properties of SBS MABs at high temperatures. Meanwhile, the increase in the LDH MAB viscosity (with 3 wt% LDHs) is also significant, increasing by 34.3% at 135 °C and 200% at 175 °C, respectively. In practical applications, 3 wt% LDH-modified asphalt has better economics due to lower raw material costs compared to 4 wt% LDH blends. Therefore, 3 wt% LDHs can ensure the adequate high-temperature performance of MABs and have the most economical values in practical applications.

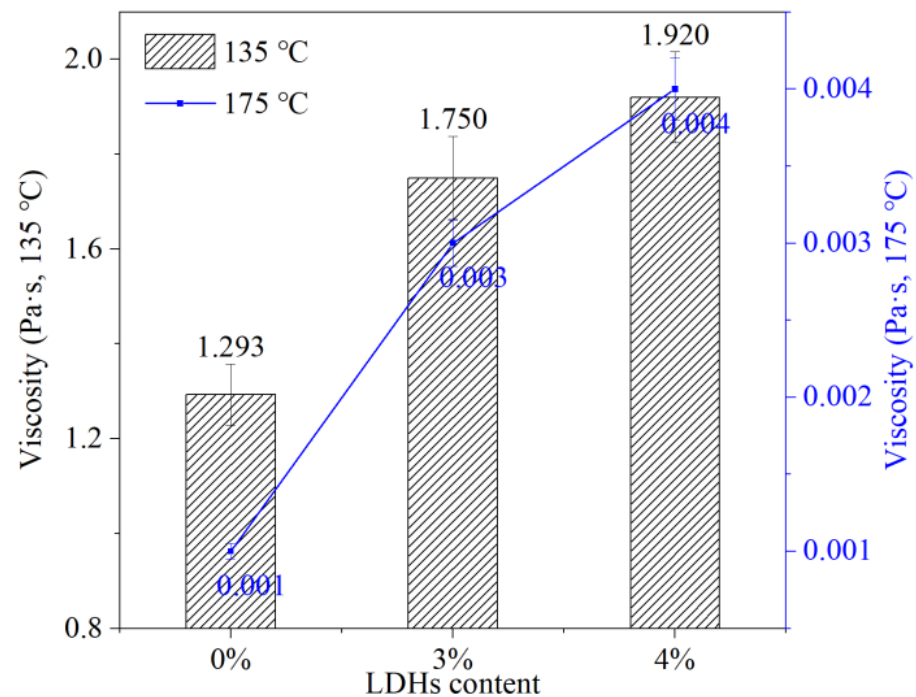


Figure 8. The viscosity of LDH MABs at 135 °C and 175 °C.

3.3. Investigation on the Anti-UV Aging Performance of LDH MABs

3.3.1. Effect of UV Aging on the Physical Properties of Aging-Resistant LDH MABs

Figure 9 displays the influence of UV aging on the PRR (%) and SPI (°C) of LDH MABs. Figure 9a shows that the PRR of SBS MABs is 49.1%, while the PRRs of the samples with 3 wt% and 4 wt% LDHs are 49.9% and 52.7%, respectively. In Figure 9b, the SPI values of the MABs doped with 3 wt% and 4 wt% LDHs are 1.2 °C and 0.9 °C, respectively, reductions of 1.1 °C and 1.4 °C compared to SBS MABs. The main reason for the change is that the light components in SBS MABs volatilize during the UV aging process, leading to a penetration decrease and softening point increase. However, the resistance of LDH MABs to UV aging is improved owing to the physical shielding and chemical absorption of UV light by LDHs, thus leading to an increase in the PRR and a decrease in the SPI. The micro- and nano-scale layered structure of LDHs, upon uniform dispersion within asphalt, engenders a heightened viscosity, consequently reducing the asphalt's flowability under elevated temperatures and thereby elevating its softening point. Additionally, SBS's ability to establish a three-dimensional network structure within asphalt, coupled with the potential interaction between LDHs and SBS within the modified asphalt, engenders a synergistic effect. This interaction further reinforces the stability of the polymer network, consequently enhancing the high-temperature deformation resistance of the modified asphalt and resulting in an increase in its softening point. Overall, with LDHs added, the PRR and SPI of LDH MABs show increasing and decreasing trends, respectively, demonstrating that the anti-UV aging performance of LDH MABs is apparently enhanced. The LDHs possess a lamellar structure that facilitates the absorption and scattering of UV light. This property serves to attenuate the incidence of UV radiation penetrating into the asphalt matrix, thereby diminishing molecular excitation and oxidation opportunities. By mitigating UV light exposure, LDHs effectively retard the aging process of asphalt.

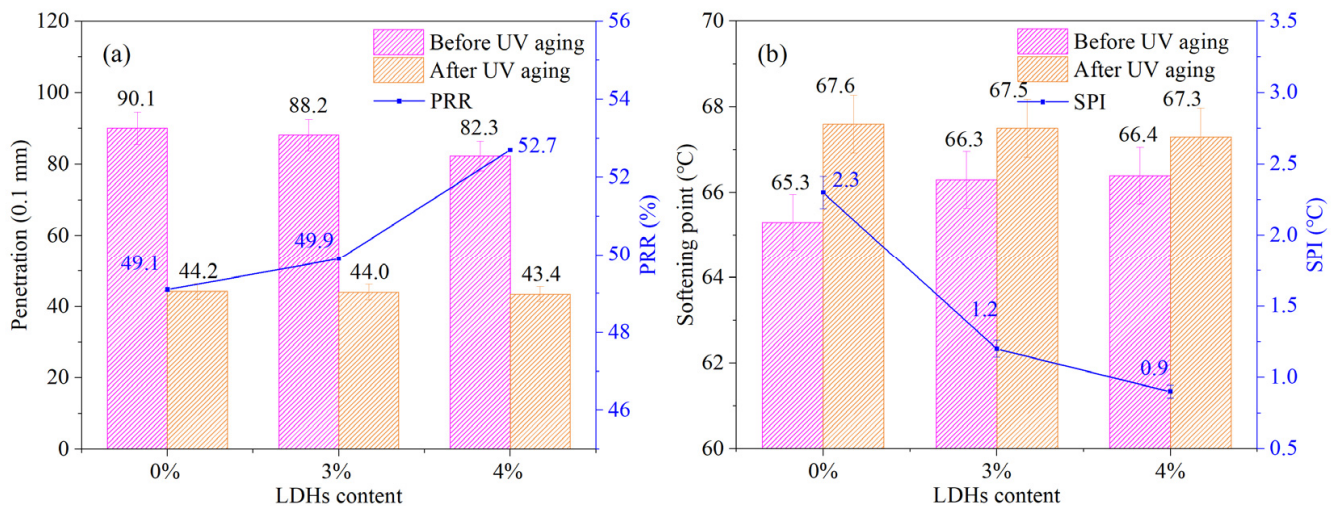


Figure 9. Effect of UV aging on (a) PRR (%) and (b) SPI (°C) of LDH MABs.

3.3.2. Effect of UV Aging on the Viscosity of Aging-Resistant LDH MABs

Figure 10 shows the effect of UV aging on the VAI of LDH MABs at 135 °C and 175 °C. The VAI reflects the aging degree of ABs. A low VAI value represents a high anti-aging performance of ABs. As can be seen from the graphs, the VAI of LDH MABs undergoes a dramatic decrease at different temperatures compared to SBS MABs. For instance, the VAI of SBS MABs is 24.5% at 135 °C, while the VAI values of the samples with 3 wt% and 4 wt% LDHs are 7.9% and 7.6%, respectively. The difference is because the reflection and absorption of UV light by LDHs notably enhance the anti-UV aging performance of LDH MABs.

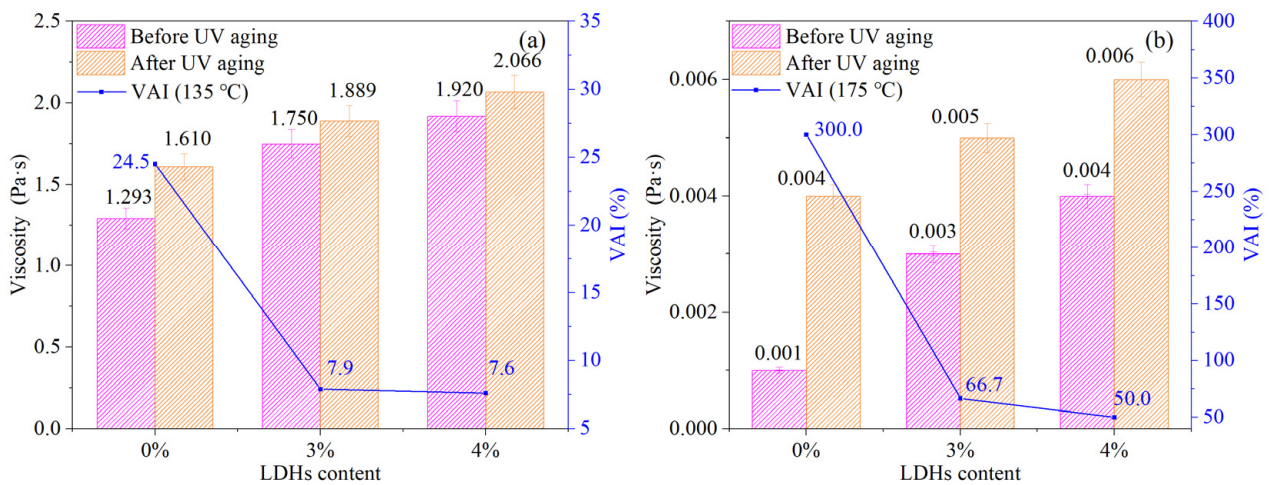


Figure 10. Effect of UV aging on the VAI (%) of LDH MABs ((a) 135 °C, (b) 175 °C).

3.3.3. Effect of UV Aging on the Rheological Properties of Aging-Resistant LDH MABs

(1) Low-temperature rheological performance

The low-temperature rheological performance of LDH MABs is investigated using the modulus of the shear strength parameter (S) and the slope of the consistency parameter (m -value). The S reflects the resistance of the asphalt to deformation at low temperatures, while the m -value represents the sensitivity of creep strength to time. The ABs with a low S and a high m -value have preferable performances at low temperatures. The American SHRP specifies an S of no more than 300 MPa and an m -value of no less than 0.300. Both the S and m -values of unaged and UV-aged LDH MABs at -12 °C and -18 °C are reported in Figure 11.

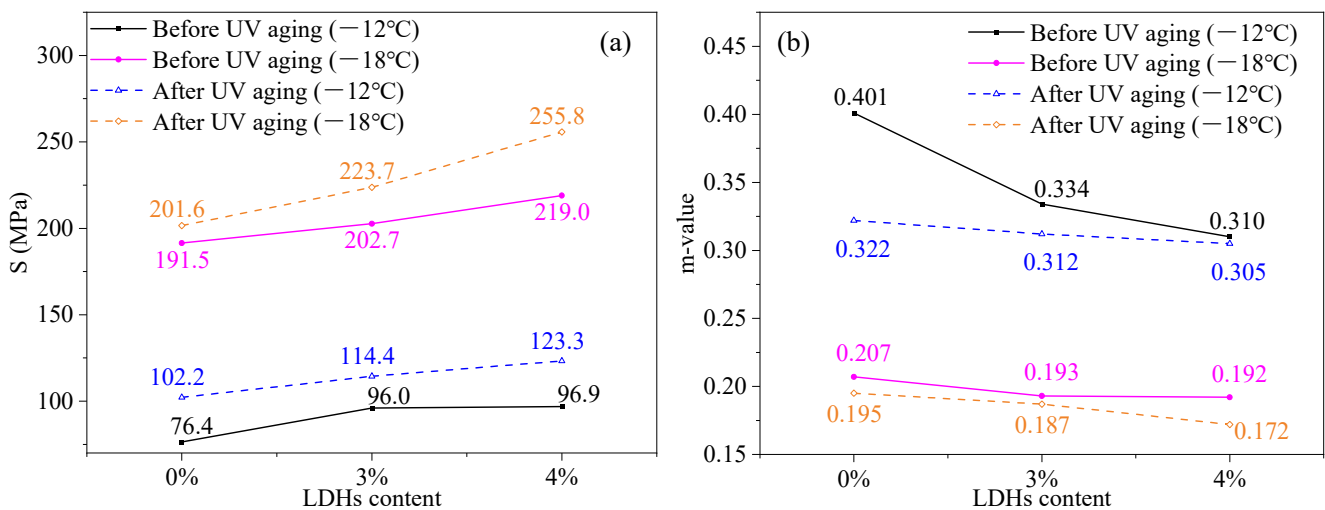


Figure 11. Low-temperature rheological properties of LDH MABs ((a) S , (b) m -value).

The introduction of micro- and nano-scale LDH particles leads to a non-uniform dispersion within the asphalt matrix. This can result in these particles becoming rigid barriers at low temperatures, impeding the movement and rearrangement of asphalt molecules. Consequently, the overall rigidity of the asphalt increases, leading to heightened low-temperature brittleness. With the LDH content increasing or the temperature decreasing, the S and m -value slightly increase and decrease, respectively, but are still within the range required by SHRP. This suggests that the impact of LDHs on the low-temperature performance of ABs is modest. After UV aging, the S of the specimens obviously increases,

and the m -value decreases significantly. However, the addition of LDHs suppressed the negative impact of UV aging on the low-temperature performance of ABs. For instance, the S and m -value of SBS MABs before UV aging were 76.4 MPa and 0.401, respectively, which changed into 102.2 MPa and 0.322, respectively, after UV aging, with an increase in the S of 33.8% and a decrease in the m -value of 19.7%. Nevertheless, the increase in the S for the MABs doped with 3 wt% LDHs was only 19.2%, and the decrease in the m -value was just 6.6% under the same UV aging conditions. It indicates that the addition of LDHs markedly enhances the crack resistance of the UV-aged ABs at low temperatures.

(2) Low-temperature cracking performance

The distresses of asphalt pavement at low temperatures can seriously affect the road performance of asphalt mixtures, especially low-temperature cracking [39,40]. A DTT was therefore conducted at $-20\text{ }^{\circ}\text{C}$ to investigate the cracking resistance of MABs at low temperatures. Three significant parameters of the DTT, including the peak force (PF), peak displacement (PD), and fracture energy (FE), are presented in Figure 11. MABs with higher PF, PD, and FE values have higher critical stress values and toughness at low temperatures, among which the FE value has the strongest comprehensive evaluation significance.

Figure 12a–c show that the FE values of all samples before UV aging are relatively high, and SBS MABs have the highest FE value of 4873 J/m^2 , showing the best low-temperature cracking resistance. In comparison, the FE values of MABs doped with 3 wt% and 4 wt% LDHs are 4518 J/m^2 and 4248 J/m^2 , respectively, just 7.3% and 12.8% lower than those of ABs without LDHs. This illustrates that the incorporation of LDHs has a minor impact on the cracking performance of SBS MABs at low temperatures.

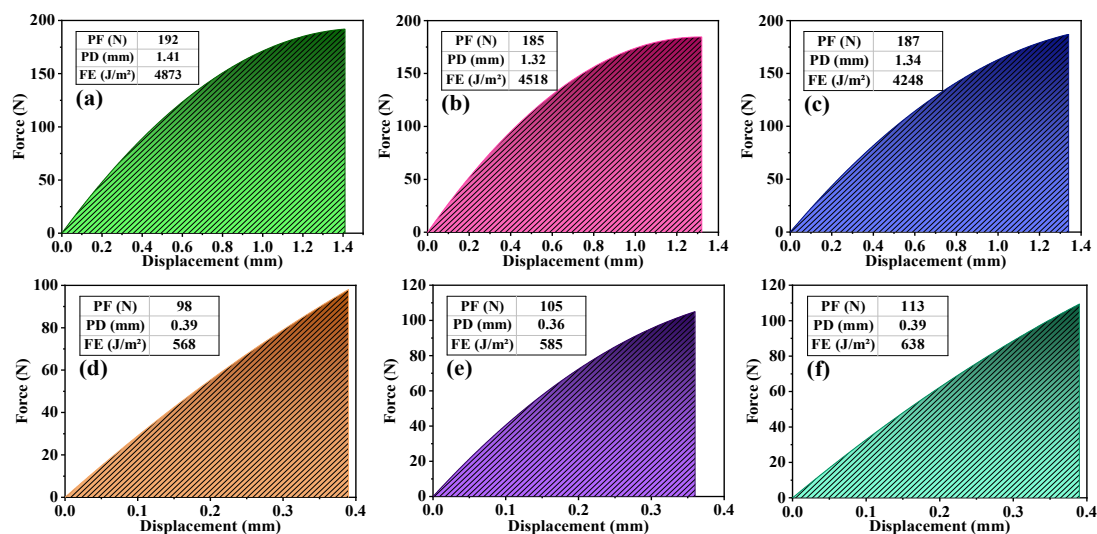


Figure 12. DTT results of all binders ((a) SBS MAB, (b) SBS + 3 wt% LDH MAB, (c) SBS + 4 wt% LDH MAB; (d) SBS MAB-UV, (e) SBS + 3 wt% LDH MAB-UV, (f) SBS + 4 wt% LDH MAB-UV).

As can be observed from Figure 12d–f, the FE values of the aged SBS MABs, 3 wt% LDH MABs, and 4 wt% LDH MABs dramatically decrease to 568 J/m^2 , 585 J/m^2 , and 638 J/m^2 , respectively, indicating that the low-temperature behavior of UV-aged binders is fragile. This is because the heavy components of the ABs increase after UV aging, decreasing the low-temperature performance. However, the reductions in SBS MABs, 3 wt% LDH MABs, and 4 wt% LDH MABs are 88.3%, 87.1%, and 85.0%, respectively; that is, the SBS MABs own the highest FE value, showing the lowest UV aging resistance. Hence, incorporating LDHs enhances the UV aging resistance of SBS MABs, and the enhancement effect grows with the amount of doping.

(3) Intermediate-temperature rheological performance

The rheological properties of unaged and UV-aged specimens at intermediate temperatures were investigated using a DSR test (40–88 °C), and the complex modulus (G^*), phase angle (δ), and rutting factor ($G^*/\sin \delta$) were obtained. Figure 13a displays the influence of LDHs on the G^* of unaged and UV-aged ABs. The G^* value of MABs continues to decrease as the temperature increases; that is, their resistance to external deformation becomes weaker. Compared with SBS MABs, the G^* of LDH MABs is higher, showing a superior resistance to external deformation than that of the former. The variation range of MABs is in the following order: SBS > SBS + 3 wt% LDHs > SBS + 4 wt% LDHs, indicating that the SBS MABs with 3 wt% LDHs have the best anti-UV aging performance.

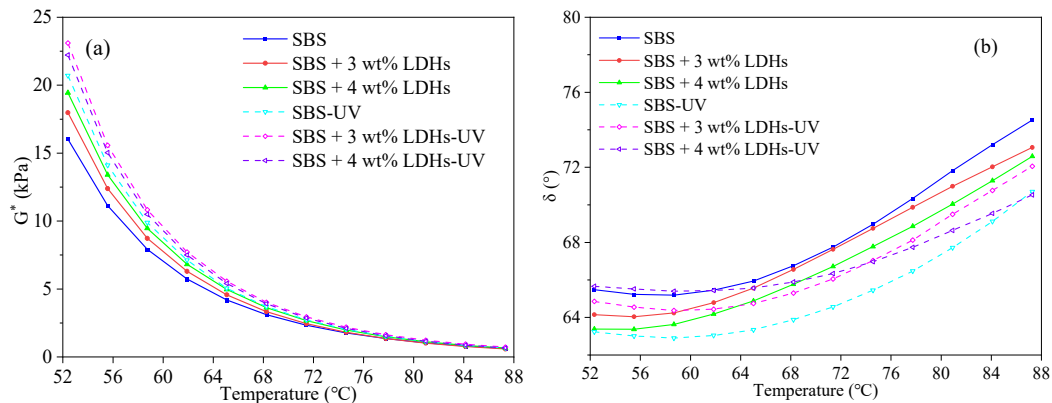


Figure 13. High-temperature rheological properties of LDH MABs with different LDH contents ((a) complex modulus, (b) phase angle).

Figure 13b details that the δ value increases as the temperature increases. With LDHs added, the δ value of unaged samples decreases and reaches the minimum when the LDH content is 4 wt%. This is mainly because of the hindering effect of LDHs on the movement of asphalt molecules. However, the δ values of all UV-aged specimens are lower than those of the unaged samples. This is because the viscous behavior of the AB gradually transforms into elastic behavior, leading to the decrease in the δ value. And the rangeability of the aged specimens' δ values in descending order is SBS > SBS + 4 wt% LDHs > SBS + 3 wt% LDHs. The LDH MABs (with 3 wt% LDHs) show the least variation in the δ value after UV aging; that is, the 3 wt% LDHs suppress the reduction in the phase angle δ the most. Thus, compared with SBS MABs and 4 wt% LDH MABs, 3 wt% LDH MABs own the best UV aging resistance, which can mainly be ascribed to the optimal dispersion of 3 wt% LDHs in the AB.

The influence of LDH content on the CMAI is shown in Table 4. A higher CMAI value indicates a greater extent of volatilization of lighter components from the modified asphalt upon exposure to ultraviolet radiation, thereby signifying more pronounced UV aging. As observed from Table 4, substantial increases in LDH dosage substantially diminish the CMAI index of the modified asphalt. This pronounced effect primarily stems from LDHs' capacity for free radical scavenging, interface protection, and antioxidative action within the modified asphalt matrix, which collectively enhance the material's UV aging resistance.

Table 4. The CMAI of LDH MABs with different LDH contents.

LDH Content	CMAI
0%	30.2%
3%	21.9%
4%	14.3%

3.3.4. Effect of UV Aging on the Chemical Properties of Aging-Resistant LDH MABs

The chemical structure of asphalt changes during UV aging. The content of the characteristic functional groups of MABs is analyzed using FTIR to determine the aging

degree. The FTIR spectra of aged and unaged MABs are shown in Figure 14. During aging, the relative content of oxygen-containing functional groups, such as carbonyl (C=O) and sulfoxide groups (S=O), increases in MABs because of the absorption of oxygen. The relative contents of C=O (RCC) and sulfoxide groups (RCS) are therefore used to evaluate the aging degree of MABs, as shown in Equations (6) and (7).

$$\text{RCC} = \frac{S_{1700 \text{ cm}^{-1}}}{S_{2000 \text{ cm}^{-1} \sim 600 \text{ cm}^{-1}}} \quad (6)$$

$$\text{RCS} = \frac{S_{1030 \text{ cm}^{-1}}}{S_{2000 \text{ cm}^{-1} \sim 600 \text{ cm}^{-1}}} \quad (7)$$

where $S_{1700 \text{ cm}^{-1}}$ and $S_{1030 \text{ cm}^{-1}}$ represent the absorption bands area of C=O and S=O, respectively, and $S_{2000 \text{ cm}^{-1} \sim 600 \text{ cm}^{-1}}$ represents that of all functional groups between 2000 cm^{-1} and 600 cm^{-1} .

The RCC and RCS for all aged and unaged MABs are presented in Figure 15. Both RCC and RCS values of the binders increase after UV aging. However, in Figure 15a, the RCC value of aged MABs decreases with the addition of LDHs. Compared to SBS MABs, the rangeability of RCC for 3 wt% and 4 wt% LDH MABs is reduced by 47% and 103%, respectively, showing the prominent restraint of LDHs on the UV aging of asphalt. The metal ions present within LDHs can act as catalysts, facilitating beneficial chemical processes, including self-reduction. These catalytic activities may suppress oxidative reactions triggered by UV radiation, thereby safeguarding the integrity of asphalt components against oxidation-induced degradation. Under UV irradiation, free radicals are generated, which are highly reactive and capable of initiating oxidative reactions leading to asphalt aging. LDHs function as scavengers for these free radicals, intercepting their reactivity and reducing the rate of oxidative reactions induced by UV radiation. This scavenging action contributes to the deceleration of asphalt aging. More notably, the RCS values for MABs with 3 wt% and 4 wt% LDHs are 1.7% and 1.5%, respectively, significant reductions of 13.4% and 13.6% compared to the 15.1% of SBS MABs. This indicates that LDHs can remarkably enhance the UV aging resistance of SBS MABs.

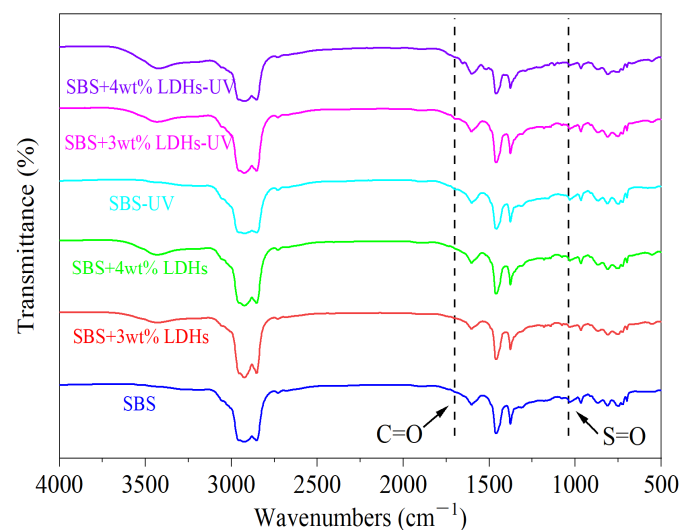


Figure 14. The FTIR spectra of MABs before and after UV aging.

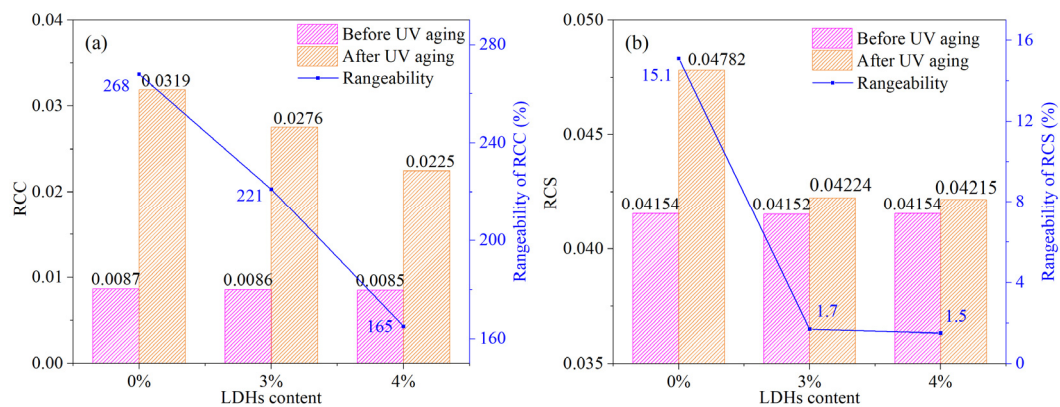


Figure 15. The RCC and RCS of MABs before and after UV aging ((a) RCC, (b) RCS).

4. Conclusions

This paper investigated the influence of the specific preparation parameters and the LDH content on the physical, rheological, and anti-UV aging performance of LDHs + SBS MABs. FTIR, XRD, and SEM were also utilized to determine the chemical and crystalline structure of LDHs and D-LDHs. The following conclusions can be drawn:

- (1) FTIR, XRD, and SEM results demonstrate that the structure of LDHs remained unchanged before and after use in asphalt modification. This means that LDHs have stable physical and chemical properties under the preparation conditions in this paper, which can confirm their preeminent anti-UV properties in engineering applications.
- (2) The optimal preparation parameters are a preparation temperature of 170 °C, shearing time of 60 min, and shearing rate of 4000 r/min. And the optimal doping of LDHs is 3 wt%. Under this condition, the low-temperature properties of LDHs + SBS MABs partially decrease, while the high-temperature performance increases significantly. Noticeably, the softening point of LDHs + SBS MABs increases immensely, which is 28.8% higher than that of SBS MABs. And 3 wt% LDHs + SBS MABs have the best high-temperature storage stability.
- (3) LDHs significantly affect MABs, and the aging index (PRR, SPI, and VAI) and FTIR results demonstrate that the UV aging resistance of LDHs + SBS MABs grows with the LDHs added. Compared with SBS MABs, the RCC and RCS rangeability of 3 wt% LDHs + SBS MABs are reduced by 47% and 13.4%, respectively, demonstrating a significant enhancement in anti-UV aging performance.
- (4) The results of the BBR, DTT, and DSR indicate that the rheological properties of LDHs + SBS MABs obtained under the optimal preparation conditions are markedly improved at high temperatures, and LDHs have a positive effect on the low-temperature performance of the UV-aged binders. After UV aging, the S of SBS MABs increases by 33.8%, and the m-value decreases by 19.7%, while those of the ABs doped with 3 wt% LDHs are just 19.2% and 6.6%, showing a preferable anti-UV aging performance.
- (5) LDHs have stable physical and chemical properties; LDHs + SBS MABs, obtained with the optimal preparation parameters, have a fine anti-UV aging performance and adequate high- and low-temperature rheological properties and thus have meaningful reference values for practical engineering applications. The results of this study on the optimal preparation parameters of LDHs + SBS-modified asphalt are of great significance for practical engineering applications, and the results of this study on the performance of modified asphalt with different LDH dosages provide a guiding basis for the design of asphalt pavements.

Author Contributions: Conceptualization, S.W.; Formal analysis, Y.S.; Investigation, Y.S. and A.C.; Methodology, Y.S., S.W. and A.C.; Project administration, S.W. and Y.L.; Resources, Y.L.; Supervision, A.C. and Y.L.; Writing—original draft, Y.S. and Y.L.; Writing—review and editing, S.W. and A.C. All authors have read and agreed to the published version of the manuscript.

Funding: This research was funded by National Key R&D Program of China: 2018YFB1600200; Hubei Science and Technology Innovation Talent and Service Project (International Science and Technology Cooperation): 2022EHB006; Key R&D Program of Guangxi Province: 2021AB26023; National Natural Science Foundation of China: 52108415; State Key Laboratory of Silicate Materials for Architectures of (Wuhan University of Technology): SYSJJ2022-21; the Open Funding of Engineering Research Center of Ministry of Education for Traffic Pavement Materials: 300102312501; the Fundamental Research Funds for the Central Universities, CHD, the Fujian Provincial Science and Technology Planning Project: 2022H0027.

Acknowledgments: The authors acknowledge the financial support from the National Key R&D Program of China (No. 2018YFB1600200), Hubei Science and Technology Innovation Talent and Service Project (International Science and Technology Cooperation) (2022EHB006), Key R&D Program of Guangxi Province (No. 2021AB26023), Beijing Xinqiao Technology Development Co., Ltd., National Natural Science Foundation of China (No. 52108415), State Key Laboratory of Silicate Materials for Architectures of Wuhan University of Technology (No. SYSJJ2022-21), Open Funding of Engineering Research Center of the Ministry of Education for Traffic Pavement Materials, Chang'an University (No. 300102312501), Fundamental Research Funds for the Central Universities, CHD, and Fujian Provincial Science and Technology Planning Project (No. 2022H0027). All individuals have consented to the acknowledgement.

Conflicts of Interest: The authors do not have any conflict of interest with other entities or researchers.

References

1. Liu, C.; Zhao, B.; Xue, Y.; He, Y.; Ding, S.; Wen, Y.; Lv, S. Synchronous method and mechanism of asphalt-aggregate separation and regeneration of reclaimed asphalt pavement. *Constr. Build. Mater.* **2023**, *378*, 131127. [[CrossRef](#)]
2. Xing, C.; Li, M.; Liu, L.; Lu, R.; Liu, N.; Wu, W.; Yuan, D. A comprehensive review on the blending condition between virgin and RAP asphalt binders in hot recycled asphalt mixtures: Mechanisms, evaluation methods, and influencing factors. *J. Clean. Prod.* **2023**, *398*, 136515. [[CrossRef](#)]
3. Wang, C.; Wang, M.; Chen, Q.; Zhang, L. Basic performance and asphalt smoke absorption effect of environment-friendly asphalt to improve pavement construction environment. *J. Clean. Prod.* **2022**, *333*, 130142. [[CrossRef](#)]
4. Zahoor, M.; Nizamuddin, S.; Madapusi, S.; Giustozzi, F. Sustainable asphalt rejuvenation using waste cooking oil: A comprehensive review. *J. Clean. Prod.* **2021**, *278*, 123304. [[CrossRef](#)]
5. Zhuang, C.Y.; Li, N.; Zhao, W.; Cai, C.F. Iop, Effects of SBS Content on the Performance of Modified Asphalt. In Proceedings of the 2nd International Conference on Civil Engineering and Materials Science (ICCEMS), Seoul, Republic of Korea, 26–28 May 2017.
6. Mo, Z. Study on the performance and aging low temperature performance of GO/SBS modified asphalt. *Matéria* **2023**, *28*, e20230151. [[CrossRef](#)]
7. Ameli, A.; Khabbaz, E.H.; Babagoli, R.; Norouzi, N.; Valipourian, K. Evaluation of the effect of carbon nano tube on water damage resistance of Stone matrix asphalt mixtures containing polyphosphoric acid and styrene butadiene rubber. *Constr. Build. Mater.* **2020**, *261*, 119946. [[CrossRef](#)]
8. Si, J.; Wang, J.; Yu, X.; Ding, G.; Ruan, W.; Xing, M.; Xie, R. Influence of thermal-oxidative aging on the mechanical performance and structure of cold-mixed epoxy asphalt. *J. Clean. Prod.* **2022**, *337*, 130482. [[CrossRef](#)]
9. Zhang, H.; Chen, Z.; Xu, G.; Shi, C. Evaluation of aging behaviors of asphalt binders through different rheological indices. *Fuel* **2018**, *221*, 78–88. [[CrossRef](#)]
10. Li, J.; Yang, J.; Liu, Y.; Zhenxia, Z.; Tang, X.; Luo, J. Fabrication of IPDI-LDHs/SBS modified asphalt with enhanced thermal aging and UV aging resistance. *Constr. Build. Mater.* **2021**, *302*, 124131. [[CrossRef](#)]
11. Ma, F.; Zhu, C.; Fu, Z.; Li, C.; Hou, Y.; Jiang, X.; Wu, M. Analysis of rheological behavior and anti-aging properties of SBS modified asphalt incorporating UV absorbent and naphthenic oil (NPO). *Constr. Build. Mater.* **2023**, *377*, 130958. [[CrossRef](#)]
12. Wu, Y.T. Low-temperature rheological behavior of ultraviolet irradiation aged matrix asphalt and rubber asphalt binders. *Constr. Build. Mater.* **2017**, *157*, 708–717. [[CrossRef](#)]
13. Yu, H.N.; Bai, X.P.; Qian, G.P.; Wei, H.; Gong, X.B.; Jin, J.; Li, Z.J. Impact of Ultraviolet Radiation on the Aging Properties of SBS-Modified Asphalt Binders. *Polymers* **2019**, *11*, 1111. [[CrossRef](#)] [[PubMed](#)]
14. Guo, M.; Yin, X.; Liang, M.; Du, X. Study on effect of thermal, oxidative and ultraviolet coupled aging on rheological properties of asphalt binder and their contribution rates. *Int. J. Pavement Eng.* **2023**, *24*, 2239426. [[CrossRef](#)]
15. Zhong, Y.; Gao, Y.; Zhang, B.; Li, X.; Wang, X. Effect of ultraviolet radiation on dielectric properties of asphalt mixture. *Int. J. Pavement Eng.* **2023**, *24*, 2157004. [[CrossRef](#)]
16. Liu, L.; Liu, Z.H.; Hong, L.L.; Huang, Y. Effect of ultraviolet absorber (UV-531) on the properties of SBS-modified asphalt with different block ratios. *Constr. Build. Mater.* **2020**, *234*, 117388. [[CrossRef](#)]
17. Bhat, F.S.; Mir, M.S. A study investigating the influence of nano Al₂O₃ on the performance of SBS modified asphalt binder. *Constr. Build. Mater.* **2021**, *271*, 121499. [[CrossRef](#)]

18. Zhao, Z.G.; Wu, S.P.; Liu, Q.T.; Yang, C.; Zou, Y.X.; Wan, P. Feasibility assessment of CeO₂ nanoparticles as aging-resistant agent of asphalt. *Constr. Build. Mater.* **2022**, *330*, 127245. [[CrossRef](#)]
19. Liu, H.B.; Zhang, Z.Q.; Xie, J.Q.; Gui, Z.J.; Li, N.Q.; Xu, Y.F. Analysis of OMMT strengthened UV aging-resistance of Sasobit/SBS modified asphalt: Its preparation, characterization and mechanism. *J. Clean. Prod.* **2021**, *315*, 128139. [[CrossRef](#)]
20. Li, X.; Wang, Y.M.; Wu, S.J.; Wang, H.R.; Liu, X.C.; Sun, H.D.; Fan, L. Effect of montmorillonite modification on resistance to thermal oxidation aging of asphalt binder. *Case Stud. Constr. Mater.* **2022**, *16*, e00971. [[CrossRef](#)]
21. Li, J.S.; Yu, J.Y.; Wu, S.P.; Pang, L.; Amirkhanian, S.; Zhao, M.L. Effect of inorganic ultraviolet resistance nanomaterials on the physical and rheological properties of bitumen. *Constr. Build. Mater.* **2017**, *152*, 832–838. [[CrossRef](#)]
22. Pizzoferrato, R.; Richetta, M. Layered Double Hydroxides (LDHs). *Crystals* **2020**, *10*, 1121. [[CrossRef](#)]
23. Crucho, J.; Neves, J. Effect of Nano Hydrotalcite on the Aging Resistance of a High Binder Content Stone Mastic Asphalt. *Appl. Sci.* **2021**, *11*, 9971. [[CrossRef](#)]
24. Ma, L.; Wang, F.; Cui, P.; Yunusa, M. Effect of aging on the constitutive models of asphalt and their mixtures. *Constr. Build. Mater.* **2021**, *272*, 121611. [[CrossRef](#)]
25. Zhang, C.L.; Chen, M.X.; Yu, M.; Wang, T.; Chen, G.C.; He, J.; Hu, C.B. Preparation of dodecyltrimethoxysilane surface organic LDHs and application in aging resistance of SBS modified bitumen. *Mater. Res. Express* **2021**, *8*, 075101. [[CrossRef](#)]
26. Xu, S.; Dang, L.; Yu, J.; Xue, L.; Hu, C.; Que, Y. Evaluation of ultraviolet aging resistance of bitumen containing different organic layered double hydroxides. *Constr. Build. Mater.* **2018**, *192*, 696–703. [[CrossRef](#)]
27. Zhao, Z.; Wu, S.; Liu, Q. Investigation of the effect of layer double hydroxides on comprehensive properties of SBS-modified asphalt mixture. *Mater. Res. Innov.* **2015**, *19*, 764–768. [[CrossRef](#)]
28. Li, Y.Y.; Wu, S.P.; Liu, Q.T.; Nie, S.; Li, H.C.; Dai, Y.; Pang, L.; Li, C.M.; Zhang, A.M. Field evaluation of LDHs effect on the aging resistance of asphalt concrete after four years of road service. *Constr. Build. Mater.* **2019**, *208*, 192–203. [[CrossRef](#)]
29. Yang, X.L.; Shen, A.Q.; Guo, Y.C.; Wu, H.S.; Wang, H. A review of nano layered silicate technologies applied to asphalt materials. *Road Mater. Pavement Des.* **2021**, *22*, 1708–1733. [[CrossRef](#)]
30. Li, R.Y.; Xiao, F.P.; Amirkhanian, S.; You, Z.P.; Huang, J. Developments of nano materials and technologies on asphalt materials—A review. *Constr. Build. Mater.* **2017**, *143*, 633–648. [[CrossRef](#)]
31. Zhang, C.; Dong, H.; Wang, T.; Li, Y.; Xu, S.; Zheng, Y.; Que, Y.; Chen, Y. Effect of different organic layered double hydroxides on the anti-aging property of bitumen. *Constr. Build. Mater.* **2023**, *367*, 130316. [[CrossRef](#)]
32. Huang, Y.F.; Feng, Z.G.; Zhang, H.L.; Yu, J.Y. Effect of Layered Double Hydroxides (LDHs) on Aging Properties of Bitumen. *J. Test. Eval.* **2012**, *40*, 734–739. [[CrossRef](#)]
33. Wang, J.S.; Wu, S.P.; Han, J.; Liu, X. Study on Preparation and UV Ageing Resistance Effect of LDHs Modified Asphalt. In Proceedings of the 3rd Mainland, Taiwan and Hong Kong Conference on Green Building Materials, Wuhan, China, 25–27 November 2011; pp. 194–202.
34. Xu, S.; Sun, Y.B.; Yu, J.Y. The Effect of Zinc Doped Mg-Al LDHs on Ultraviolet Aging Resistance of Asphalt. *Pet. Sci. Technol.* **2015**, *33*, 335–343. [[CrossRef](#)]
35. JTGE20-2011; Standard Test Methods of Bitumen and Bituminous Mixtures for Highway Engineering. Ministry of Transport of the People's Republic of China: Beijing, China, 2011.
36. Hou, X.; Lv, S.; Chen, Z.; Xiao, F. Applications of Fourier transform infrared spectroscopy technologies on asphalt materials. *Measurement* **2018**, *121*, 304–316. [[CrossRef](#)]
37. Tao, X.; Shi, L.S.; Sun, M.J.; Li, N. Synthesis of lignin amine asphalt emulsifier and its investigation by online FTIR spectrophotometry. *Adv. Mater. Res.* **2014**, *909*, 72–76. [[CrossRef](#)]
38. Li, Y.; Wu, S.; Dai, Y.; Pang, L.; Liu, Q.; Xie, J.; Kong, D. Investigation of sodium stearate organically modified LDHs effect on the anti aging properties of asphalt binder. *Constr. Build. Mater.* **2018**, *172*, 509–518. [[CrossRef](#)]
39. Cao, Z.; Chen, M.; He, B.; Han, X.; Yu, J.; Xue, L. Investigation of ultraviolet aging resistance of bitumen modified by layered double hydroxides with different particle sizes. *Constr. Build. Mater.* **2019**, *196*, 166–174. [[CrossRef](#)]
40. Lin, Q.; Zhang, Z.-Q.; Sha, A.-M.; Yang, H. Research on relationship between aging state and low-temperature performance of asphalt mixture. *J. Test. Eval.* **2009**, *37*, 486–489.

Disclaimer/Publisher's Note: The statements, opinions and data contained in all publications are solely those of the individual author(s) and contributor(s) and not of MDPI and/or the editor(s). MDPI and/or the editor(s) disclaim responsibility for any injury to people or property resulting from any ideas, methods, instructions or products referred to in the content.